Numerical simulation of the flow around the helicopter blade in hover using the MRF method and turbulence models

T. Azzam, T. Belmerabet, M. Mekadem, S. Djellal & S. Hanchi
Laboratory of Fluid Mechanics, EMP, Algiers, Algeria

Abstract

The aim of this study is to find the most adequate numerical model to simulate the aerodynamics of the helicopter rotor in hovering flight, using CFD code Fluent. In this work, the Caradonna and Tung blades are used with NACA0012 profile and an aspect ratio of six. The rotating rotor is modeled by the multiple references rotating frame method (MRF). Using the periodicity condition, computations are carried only on one blade. For grid generation, the structured mesh is generated near the wall region with $30 < y^+ < 300$ and for the rest of the computational domain, the unstructured mesh is used. The value of the near-wall resolution y_p depends on the value of the mean skin friction coefficient $\overline{C_f}$. According to the study of Lombardi et al. (Numerical Evaluation of Airfol Friction Drag. *Journal of Aircraft,* 2000), the value of $\overline{C_f}$ can be considered similar for both flat plat and NACA0012 airfoil. To evaluate the surface pressure distributions, we have treated the effect of the collective pitch angle (θ), the tip Mach number (M_{tip}) and the two turbulence models, standard $k-\varepsilon$ and Spalart-Allmaras. The obtained results are expressed in terms of pressure coefficient C_p, have been validated by comparisons with the experimental data. In addition, we discuss in this study the prediction of shock location on the upper surface of the blade.

Keywords: aerodynamic, helicopter blade, MRF, hovering flight, pressure coefficient, shock wave.

WIT Transactions on The Built Environment, Vol 115, © 2011 WIT Press
www.witpress.com, ISSN 1743-3509 (on-line)
doi:10.2495/FSI110261

1 Introduction

The CFD analysis of the flow around the rotor helicopter is particularly complicated. In hover or forward flight, the rotor operates in its own wake, characterized by three-dimensional unsteady structures and thus affecting the aerodynamics of the blade [4]**.** Starting from Navier–Stokes equations, and using advanced computing resources, we can represent with a fairly good fidelity the major feature of the viscous flow develops around the rotor [5]. However, this requires advanced computing resources. To reduce the computing time, most studies suggest, the periodicity of the flow using periodic condition.

In this work, we employed the periodic condition to simulate the flow around one blade. The motion of the blade is modeled by the multiple references rotating frame method (MRF) [6].

2 Numerical methodology

Generally, **FLUENT** solves the equations of fluid flow and heat transfer, by default, in a stationary (or inertial) reference frame. However, there are many problems where it is advantageous to solve the equations in a moving (or non-inertial) reference frame. Such problems typically involve moving parts (such as rotating blades, impellers, and similar types of moving surfaces), and it is the flow around these moving parts that is of interest. In most cases, the moving parts render the problem unsteady when viewed from the stationary frame. With a moving reference frame, however, the flow around the moving part can (with certain restrictions) be modeled as a steady-state problem with respect to the moving frame. Multiple Reference Frame method (MRF) is steady-state approximation. The flow in each moving cell zone is solved using the moving reference frame equations. If the zone is stationary ($\Omega = 0$), the stationary equations are used. At the interfaces between cell zones, a local reference frame transformation is performed to enable flow variables in one zone to be used to calculate fluxes at the boundary of the adjacent zone [6].

This study computes the steady viscous flow-fields over one blade by solving the Navier–Stokes equations using MRF method. For the solution controls, the coupled algorithm was used for the coupling between the pressure and the velocity. For the discretization schemes, the standard scheme was used for the pressure equation, and the second-order Upwind scheme for both the density, momentum and energy equations.

2.1 Grid generation and boundary conditions

The Caradonna and Tung [1] blade has been used for the validation of our numerical modeling. The blade is untwisted and untapered, with a constant NACA0012 section and an aspect ratio of six. The model rotor has a diameter $D = 2.286\,\text{m}$ and at chord length $c = 0.191\,\text{m}$. The experimental study of Caradonna and Tung involved simultaneous blade pressure measurements and tip vortex surveys. For the first case, they treated the affect of the pitch angle θ

(from 0° to 12°) and the tip Mach number M_{tip} (from 0.226 to 0.890) on the surface pressure distribution at five rotor blade sections $(r/R = 0.5, 0.68, 0.80, 0.89 \text{ and } 0.96)$. Figure 1 shows limits in term of radial station r/R of the blade used in our simulation $(r/R = 0.1 \text{ and } r/R = 1)$.

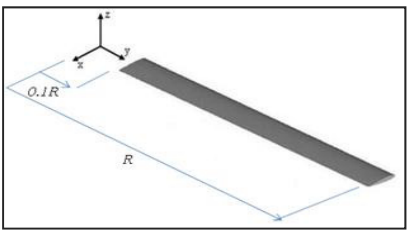

Figure 1: Caradonna and Tung rotor blade.

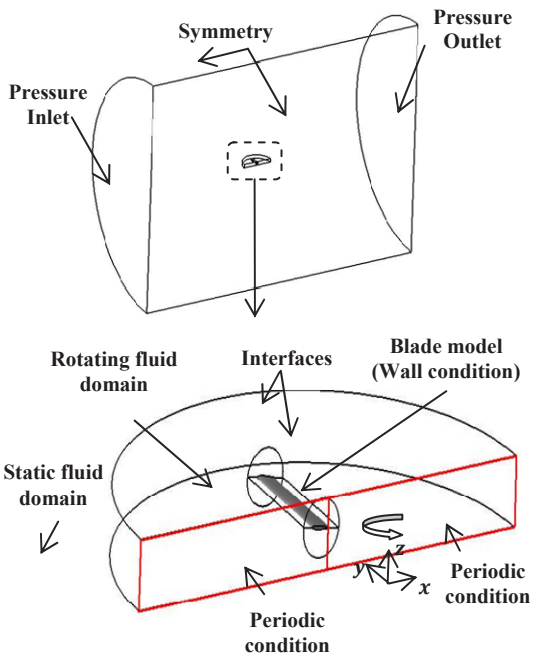

Figure 2: Boundary conditions used for computations.

We first create the geometry and computational domain using the software *Gambit*. The blade is contained in a cylindrical virtual volume which is also contained in a half virtual disk. This volume consists of the rotating domain. The rest of the computed domain remains static. We use the interface condition to

separate the moving and static domain. Due to the symmetry presented in hovering flight, periodic conditions have been employed to simulate only one blade. Figure 2 shows boundary conditions used near and far from the blade model.

For grid generation, the structured mesh is generated near the wall region with $30 < y^+ < 300$ and for the rest of the computational domain, the unstructured mesh is used. Figure 3 shows the projection of the tridimensional mesh in the *x–z* plane $(r / R = 0.8)$.

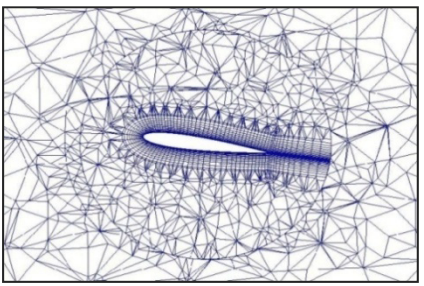

Figure 3: Projection of the mesh in the plane $r / R = 0.8$.

To estimate the near wall refinement y_p(first distance from a point (p) to the wall), first, we have the nondimensional parameter y^+ is given by the eqn (1) [6]:

$$y^+ = \frac{y_p u_\tau}{\nu} \tag{1}$$

where ν is the kinetic viscosity and u_τ is the friction velocity given by [6]:

$$u_\tau = \sqrt{\frac{\tau_w}{\rho}} = V_r \sqrt{\frac{\overline{C_f}}{2}} \tag{2}$$

τ_w is the skin friction drag and $V_r = r\Omega$ is the velocity in hovering flight.

Note that the value of the near-wall resolution y_p depends on the value of the mean skin friction coefficient $\overline{C_f}$. We have used the approximation given by Lombardi and al [2] to evaluate $\overline{C_f}$ and to estimate the value of y_p. According to the study of the Lombardi et al., the mean skin friction of flat plat and NACA0012 airfoil are similar. In other way, for turbulent flow over flat plate with Reynolds number Re, we have [3]**:**

$$\frac{\overline{C_f}}{2} = \frac{0.037}{Re^{1/5}} \tag{3}$$

2.2 Grid sensitivity test

For the test of grid sensitivity, three grid system distributions were used. Table 1 gives the total cell numbers for each grid system.

Table 1: Grid refinement test.

Grid	Cell numbers
Mesh A	162556
Mesh B	274030
Mesh C	636651

For the operating conditions, blade section $r/R = 0.8$, pitch angle $\theta = 8°$ and Tip Mach number $M_{tip} = 0.439$, figure 4 shows the distribution of C_p for the three grids with Experimental data of Caradonna and Tung study [1] (noted Exp in figure). For the upper surface of the blade, it is noted that Mesh B provided slightly identical results with Mesh C. So, Mesh B was adopted for the remaining simulation.

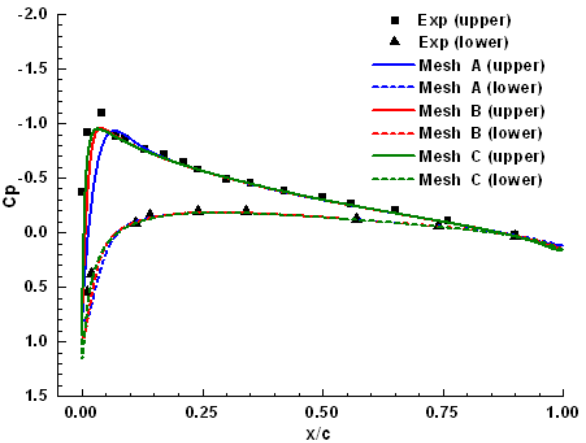

Figure 4: Surface pressure distribution $r/R = 0.8$, $\theta = 8°$, $M_{tip} = 0.439$.

3 Results and discussion

3.1 Judging convergence

There are no universal metrics for judging convergence. Residual definitions that are useful for one class of problem are sometimes misleading for other classes of problems. For most problems, the default convergence criterion in **FLUENT** is sufficient. This criterion requires that the scaled residuals decrease to 10^{-3} for all equations except the energy equation, for which the criterion is 10^{-6}. Therefore it is a good idea to judge convergence not only by examining residual levels, but

also by monitoring relevant integrated quantities such as drag or heat transfer coefficient [6]. In this work, Figure 5 confirms the two convergence criterions, where we examined the evolution of the vertical force coefficient C_l with the Spalart–Allmaras turbulent model.

$$C_l = \frac{F_l}{\frac{1}{2}\rho V_{tip}^2 A} \tag{5}$$

With F_l is the vertical force, V_{tip} is the velocity of the flow at the tip of the blade and A is the reference area.

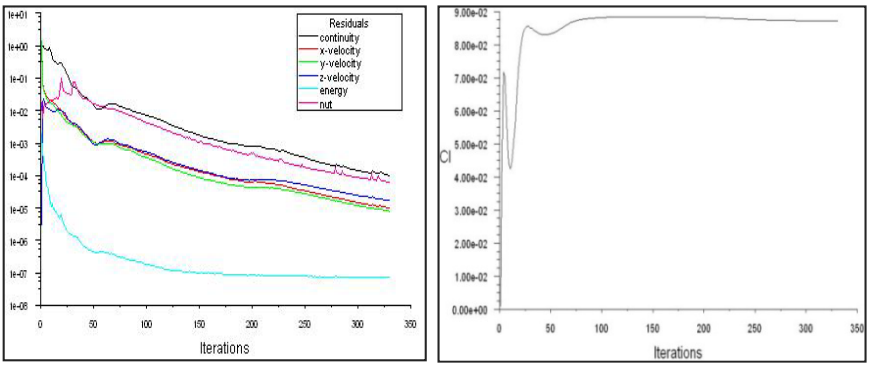

(a) (b)

Figure 5: Using the Spalart–Allmaras turbulent model, (a) residuals variations, (b) variation of C_l.

3.2 Non-lifting and lifting cases

Initially, we have considered the non-lifting case with a collective pitch angle $\theta = 0°$ and tip Mach number $M_{tip} = 0.520$. As a result, figure 6 shows the surface pressure distributions for the blade sections $(r/R = 0.80 \text{ and } 0.96)$. An excellent agreement between experimental data and results obtained with Spalart–Allmaras turbulent flow model is noted (noted SA in figures). Using the two turbulence models, standard $k-\varepsilon$ and Spalart-Allmaras, and for three radial blade sections $(r/R = 0.5,\ 0.8 \text{ and } 0.96)$, figure 7 shows the lifting case with $(\theta = 8° \text{ and } M_{tip} = 0.439)$, a disagreement between solutions at the peak of minimum of pressure coefficient. Instead of this later result, generally the present calculation gives closer agreement with experimental data.

3.3 Prediction of the shock wave

The two tests with operating parameters $(\theta = 8°,\ M_{tip} = 0.877)$ $(\theta = 12°, M_{tip} = 0.794)$ involve shock wave at the upper surface. For these two cases, figures 8 and 9 show the numerical and experimental surface pressure

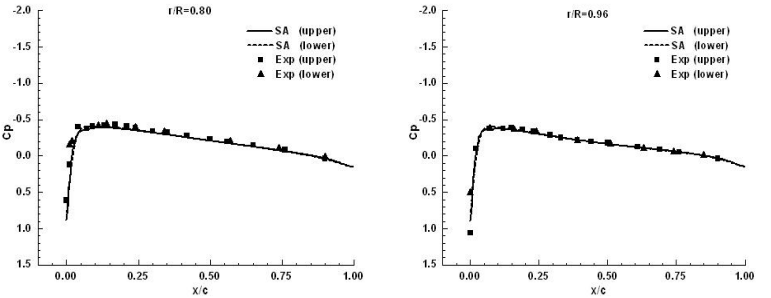

Figure 6: Surface pressure distributions $\theta = 0°, M_{tip} = 0.520$.

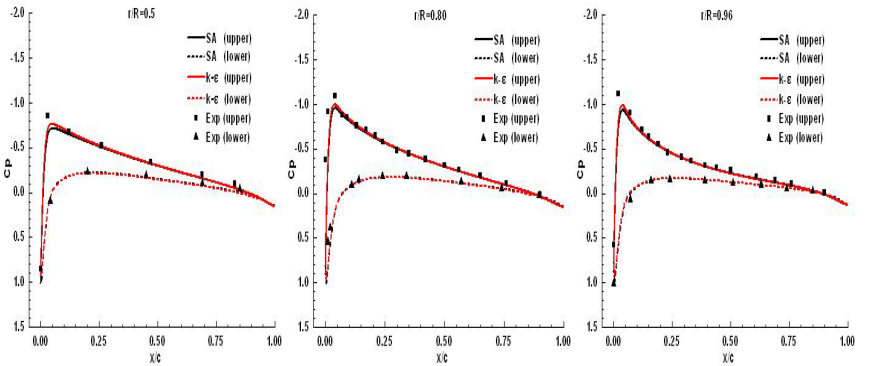

Figure 7: Surface pressure distributions $\theta = 8°, M_{tip} = 0.439$.

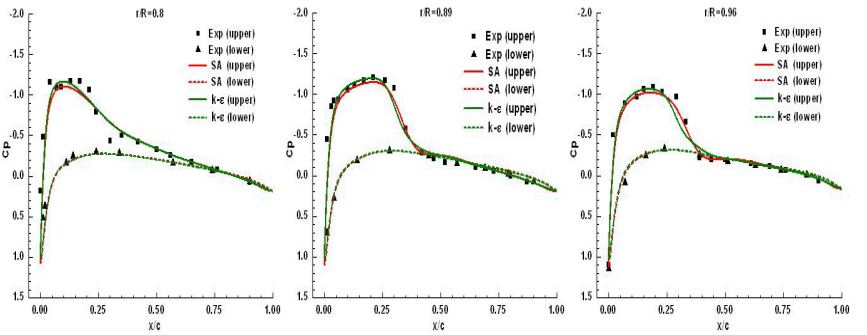

Figure 8: Surface pressure distributions $\theta = 8°,\ M_{tip} = 0.877$.

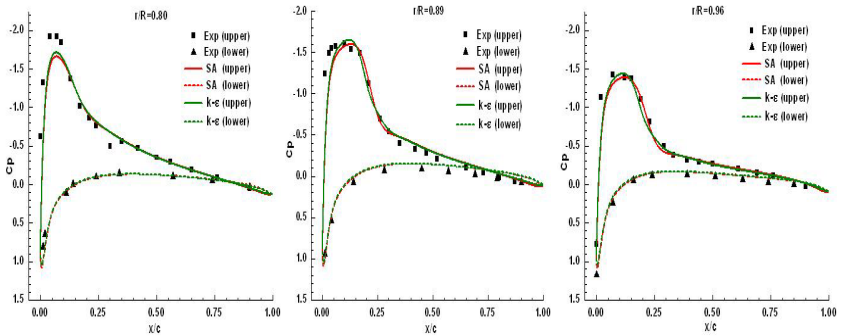

Figure 9: Surface pressure distributions $\theta = 12°,\ M_{tip} = 0.794$.

distributions for three blade sections ($r/R = 0.8,\ 0.89$ and 0.96), respectively. Generally, results were in good agreement with experiments. For the two turbulence model, there is no difference between the obtained results. A slightly better prediction for the peak of C_p has been obtained with standard $k-\varepsilon$ turbulent model. However, the location of the shock is in agreement.

4 Conclusion

A CFD framework has been presented for flow over helicopter blade in hovering flight. For this configuration of flight, the MRF method seems adequate for aerodynamic calculations of the blade.

In addition, grid refinement is also discussed by the estimation of the near-wall resolutions y_p. For the three-dimensional test cases, flow solution including surface pressure distributions and prediction of the shock location was validated against experimental data [1], with two turbulence models (standard $k-\varepsilon$ and Spalart-Allmaras), range of tip Mach numbers and pitch angles. According to the obtained results, non lifting case ($\theta = 0°,\ M_{tip} = 0.520$) shows good agreement. However, for lifting case ($\theta = 8°,\ M_{tip} = 0.439$), the peak of pressure coefficient is not captured as well.

References

[1] F.X. Caradonna, C. Tung, Experimental and analytical studies of a model helicopter rotor in hover. Technical Report. NASA Technical Memorandum 81232. 1981.

[2] G. Lombardi, M.V. Salvetti, D. Pinelli, Numerical Evaluation of Airfol Friction Drag. *Journal of Aircraft,* March-April 2000, Vol 37, No 2, pp 354-356.

[3] J.D. Anderson, *Fundamentals of Aerodynamics.* 4th Edition McGraw-Hill. 2007.

[4] A.T Conlisk, Modern helicopter rotor aerodynamics. Elsevier Science. 2001.
[5] http://www.onera.fr
[6] User's Guide: FLUENT 6.3